THE JOURNAL OF BIOLOGICAL CHEMISTRY VOL. 289, NO. 36, pp. 25374–25381, September 5, 2014

The Molecular Mechanism of Shiga Toxin Stx2e Neutralization by a Single-domain Antibody Targeting the Cell Receptor-binding Domain

Received for publication, March 20, 2014, and in revised form, July 17, 2014 Published, JBC Papers in Press, July 22, 2014, DOI 10.1074/jbc.M114.566257

Alvin W. H. Lo[‡§], Kristof Moonens[‡§1], Maia De Kerpel[‡§], Lea Brys[¶], Els Pardon[‡§2], Han Remaut[‡§3], and Henri De Greve[‡§4]

From [‡]Structural and Molecular Microbiology, Structural Biology Research Center, VIB, [§]Structural Biology Brussels, and the [¶]Laboratory of Myeloid Cell Immunology, VIB, Vrije Universiteit Brussel, Pleinlaan 2, 1050 Brussels, Belgium

Background: Swine edema disease is caused by Shiga toxin Stx2e-producing *Escherichia coli*.
Results: A potent Stx2e-neutralizing nanobody, NbStx2e1, was discovered; the crystal structure of the NbStx2e1-Stx2e complex uncovers the molecular basis of the Stx2e inhibition.
Conclusion: NbStx2e1 directly prevents the binding of Stx2e to host cell receptor.
Significance: NbStx2e1 can be employed to prevent Stx2e-mediated disease.

Shiga toxin Stx2e is the major known agent that causes edema disease in newly weaned pigs. This severe disease is characterized by neurological disorders, hemorrhagic lesions, and frequent fatal outcomes. Stx2e consists of an enzymatically active A subunit and five B subunits that bind to a specific glycolipid receptor on host cells. It is evident that antibodies binding to the A subunit or the B subunits of Shiga toxin variants may have the capability to inhibit their cytotoxicity. Here, we report the discovery and characterization of a VHH single domain antibody (nanobody) isolated from a llama phage display library that confers potent neutralizing capacity against Stx2e toxin. We further present the crystal structure of the complex formed between the nanobody (NbStx2e1) and the Stx2e toxoid, determined at 2.8 Å resolution. Structural analysis revealed that for each B subunit of Stx2e, one NbStx2e1 is interacting in a head-to-head orientation and directly competing with the glycolipid receptor binding site on the surface of the B subunit. The neutralizing NbStx2e1 can in the future be used to prevent or treat edema disease.

Shiga toxin Stx2e-producing strains of *Escherichia coli* are the major cause of edema disease (ED)[5] in newly weaned piglets. This is a disease that is highly contagious and leads to neurological disorders, hemorrhagic lesions, and frequent fatal outcome (1, 2). The structure of Stx2e holotoxin was previously determined (3), and like other Shiga toxin variants, Stx2e consists of an enzymatically active A subunit and five B subunits that bind to a specific glycolipid receptor on host cells. The A subunit confers *N*-glycosidase activity that specifically cleaves an adenosine base in the 28 S rRNA of the 60 S ribosomal subunits, inhibiting protein synthesis in target cells. The B subunits of Stx2e, on the other hand, bind to the glycolipid receptor, globotriaosylceramide (Gb3), or preferentially to globotetraosylceramide (Gb4) (4) receptors that are present in the porcine small intestine, where, through endocytosis, the holotoxin is internalized into target cells.

The high mortality rate in Stx2e-producing *E. coli*-infected pigs has had dire economic consequences for the swine industry. To date, no vaccine or effective therapeutic agent is available for the treatment of ED, and the standard treatment is the use of antibiotics. However, excessive use of antibiotics and the prevalence of antibiotic-resistant porcine Stx2e-producing *E. coli* isolates are of increasing concern, underscoring the urgent need to develop new therapeutic approaches. Recently, an immunoprophylaxis approach, where piglets and sows were immunized with a genetically inactivated Stx2e (Stx2e toxoid), showed promising results (5). Immunized piglets and pregnant sows were protected against Stx2e toxin challenge. Moreover, immunized pregnant sows provide high levels of passive antibodies in piglets (5).

It has been shown that antibodies binding to the A subunit or the B subunits of Shiga toxin variants have the capability to inhibit their cytotoxicity (6–11). Two of these monoclonal antibodies (mAbs), ShigamAbs (Thallion Pharmaceuticals) (8) and Urtoxazumab (Teijin) (12), are undergoing clinical trials. Despite the promising preclinical and early clinical results, there are several considerations to be taken into account in the development and application of these mAbs, including the difficulty and the high cost of optimization and production of mAbs, the mode and timing of delivery of mAbs, and whether they are likely to mitigate or alter the outcome of the diseases.

The promising preclinical and early clinical results of these mAbs have spurred significant interest to exploit VHH single

The atomic coordinates and structure factors (code 4P2C) have been deposited in the Protein Data Bank (http://wwpdb.org/).

[1] Doctoral fellow of the Fond voor Wetenschappelijk Onderzoek (FWO)-Vlaanderen.
[2] Supported by Grant 7/40 of the Interuniversity Attraction Poles (IAP) Program of the Belgian Science Policy Office.
[3] Supported by a VIB Young PI project grant and the Odysseus program of the FWO-Vlaanderen.
[4] To whom correspondence should be addressed: Structural and Molecular Microbiology, Structural Biology Research Center, VIB, Pleinlaan 2, 1050 Brussels, Belgium. Tel.: 32-2-629-18-44; Fax: 32-2-629-19-63; E-mail: hdegreve@vub.ac.be.
[5] The abbreviations used are: ED, edema disease; Bistris propane; 1,3-bis-[tris(hydroxymethyl)methylamino]propane; SPR, surface plasmon resonance; CDR, complementarity-determining region.

domain antibodies (nanobodies) (13) derived from camelids that possess significant advantages over conventional antibodies. While conferring high affinity and antigen specificity, the relative smaller size of the nanobodies, their high stability and solubility, and their easy and cost-effective production make them a propitious therapeutic agent (14). Moreover, the amenability of nanobodies as multivalent molecules that recognize a number of targets has significant therapeutic applications (14). Indeed, a recent study has identified nanobodies that neutralize Shiga toxin variant Stx1 and/or Stx2 (15). This study further showed that fusing multiple nanobodies that recognize the Stx1/2 B subunits results in a potent cross-specific nanobody that confers protection in mice against Shiga toxin challenge (15). The exact molecular mechanism of inhibition of this nanobody, however, remains to be established.

In this study, we described the identification and characterization of a potent Stx2e-neutralizing nanobody, NbStx2e1, and further elucidated the structural basis for its mechanism of neutralization. The co-complex structure uncovers atomic details of the NbStx2e1 paratope-epitope interactions and further shows that the neutralization of Stx2e cytotoxicity by NbStx2e1 is achieved by direct interaction with the Stx2e B subunit binding site for glycolipid, thereby impeding toxin-host cell receptor contacts.

EXPERIMENTAL PROCEDURES

Production of Stx2e Toxin, Stx2e Toxoid, and Stx2 Crude Extract—The construction, expression, and purification of Stx2e toxin and toxoid (with mutations at two amino acid positions (Y77S and E167Q) in the active site of the A subunit) were as described previously by Oanh *et al.* (5). For Stx2, total genomic DNA from *E. coli* strain C600 (933W) (16) was used as template to amplify the *stx2* operon with primers Stx2-2 (5′-GGGGACCACTTTGTACAAGAAAGCTGGGTAATG-CCTCAGTCATTATTAAACTGCACTTC-3′) and Stx2-3 (5′-GGGGACAAGTTTGTACAAAAAAGCAGGCTTAGGT-GCTGATTACTTCAGCCAAAAG-3′). The resulting PCR fragment was cloned in the pDONR221 vector using the BP reaction (Gateway Technology, Invitrogen) and transformed in $CaCl_2$-competent DH5α cells. Transformants were selected on LB medium supplemented with 25 μg/ml kanamycin and sequenced with the primers SeqLA and SeqLB (5) located in the pDONR221. A positive clone, pHD983, was selected to introduce the *stx2* operon into the expression vector pDEST14 (Gateway Technology, Invitrogen) using the LR reaction yielding pHD914. The clone harboring pHD914 was induced at 1 mM isopropyl β-D-1-thiogalactopyranoside at 37 °C. Cells were collected and suspended in PBS. The cell suspension was disrupted by sonication, and crude extract of Stx2 was clarified by centrifugation.

Ethics Statement—All animal vaccination experiments were executed in strict accordance with good animal practices, following the European Union animal welfare legislation and after approval of the local ethical committee (Committee for the Use of Laboratory Animals at the Vrije Universiteit Brussel). Every effort was made to minimize animal suffering.

Llama Immunization with Stx2e Toxoid—A llama was immunized six times with 330 μg of purified Stx2e toxoid over a period of 6 weeks. From the anti-coagulated blood of the immunized llama, lymphocytes were used to prepare cDNAs that served as a template to amplify the open reading frames coding for the variable domains of the heavy chain antibodies. The PCR fragments, encoding the open reading frames of the nanobodies, were ligated into the pMES4 (GenBank™ accession number GQ907248) phage display vector and transformed in *E. coli* TG1 cells (17). The selection of Stx2e-specific nanobodies was performed by phage display. After selection, phages were eluted by incubating the Stx2e-coated wells with 100 mM triethylamine (pH 10) for 10 min. The Stx2e-coated wells were then washed once with Tris-HCl (pH 6.8) and several times with PBS, and freshly grown TG1 cells were added to the wells to recover the non-eluted phages. After two rounds of panning, 90 individual colonies were selected and grown in 2× TY medium supplemented with ampicillin and induced with 1 mM isopropyl β-D-1-thiogalactopyranoside for expression of soluble periplasmic nanobodies. The periplasmic extract was subjected to ELISA to assess the presence of nanobodies recognizing purified Stx2e toxoid.

Expression and Purification of Stx2e-specific Nanobodies—Nanobodies were expressed and purified as described previously by Conrath *et al.* (18). Briefly, *E. coli* strain WK6 harboring plasmid encoding a nanobody bearing a C-terminal His tag was grown at 37 °C in lysogeny broth (LB) medium supplemented with 100 μg/ml ampicillin. Cells were induced at $A_{600\,nm}$ of 0.9 with 1 mM isopropyl β-D-1-thiogalactopyranoside at 28 °C overnight, and the nanobody was isolated by periplasmic extraction of cells. Nanobodies were purified using a HisTrap FF (Fast Flow) column (GE Healthcare) and subjected to a 20 mM to 1 M imidazole linear gradient in 20 mM Tris, pH 8.0, 1 M NaCl. Fractions containing the nanobody, as judged by SDS-PAGE, were pooled and dialyzed against PBS overnight at 4 °C. The purity of the isolated nanobodies was assessed in SDS-PAGE.

Enzyme-linked Immunosorbent Assay (ELISA) of Stx2e Toxoid and Nanobodies—To assess the interaction of nanobodies with Stx2e toxoid, Nunc MaxiSorp™ flat-bottom 96-well plates (eBioscience) were coated with purified Stx2e toxoid at 2 μg/ml suspended in coating buffer ($NaHCO_3$ at pH 8.4). The wells were washed three times with PBST (PBS and 0.2% (v/v) Tween 20) and blocked with 2% skimmed milk in PBS. A serial dilution of nanobodies was performed with a starting concentration for each nanobody of 20 μg/ml. The interaction of nanobodies with Stx2e toxoid was detected using a mouse monoclonal anti-histidine tag antibody (AbD Serotec) followed by alkaline phosphate-conjugated goat anti-mouse IgG (Sigma). The reaction was developed in the presence of *p*-nitrophenyl phosphate substrate (Sigma), and absorbance was read at 405 nm.

Stx2e Neutralization Assay—The Stx2e toxin-neutralizing activity of nanobodies was assessed in a Vero cell-based assay, as described previously (5). Briefly, 2-fold serial dilutions of nanobodies in PBS were performed with a starting concentration of 500 ng/ml and incubated at room temperature for 30 min in the presence of an equal volume of purified Stx2e toxin at a predetermined dilution (2 ng/ml). The Stx2e toxin/nanobody mixtures were added to wells of a 96-well plate (Falcon BD) containing a confluent culture of Vero cells (ATCC CCL-

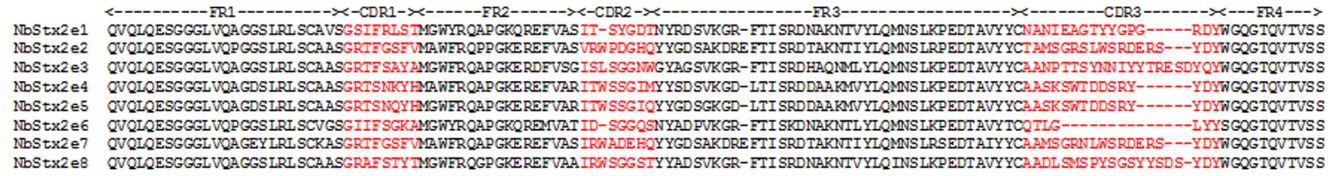

FIGURE 1. **Amino acid sequences alignment of isolated nanobodies recognizing Stx2e.** Amino acid sequence analysis revealed that these nanobodies belong to six different families, based on the CDR3 variation. *FR1–4* denote the structural framework regions, and *CDR1–3* indicate the complementarity-determining regions. The amino acid sequences are *numbered* according to IMGT numbering (38). The six-histidine residue tag at the C terminus of each nanobody has not been included in the alignment.

81) grown in Dulbecco's modified Eagle's medium, supplemented with 5% fetal bovine serum. After a 1-day incubation in a humidified incubator (5% CO_2 environment), medium was removed, and the remaining cells were fixed with 2% formaldehyde in PBS for 5 min. Cells were then stained with 0.13% (w/v) crystal violet dissolved in 5% ethanol, 0.2% formaldehyde, PBS for 5 min. Cells were washed six times with water. Cell-adsorbed crystal violet was extracted in 200 μl of 50% ethanol plus PBS, and absorbance was measured at 595 nm. Nanobody-only and toxin-only controls were included in the assays. The results were expressed as percentage viability compared with that of control Vero cells in the presence of nanobody without toxin (100% viability) and with toxin only (0% viability). The IC_{50} values were calculated by nonlinear regression analysis using GraphPad Prism.

Surface Plasmon Resonance (SPR) Measurements—SPR experiments were carried out using a Biacore 3000 instrument (GE Healthcare). The surface of a CM5 sensor chip was activated with a 1:1 mixture of 0.1 M *N*-hydroxysuccinimide and 0.4 M 1-ethyl-3-(3-dimethylamino-propyl) carbodiimide hydrochloride. After activation of the surface the Stx2e toxin (20 μg/ml) in 10 mM sodium acetate, pH 3 was injected to flow cell 2 (FC2) to be immobilized on the sensor surface via primary amine groups present on Stx2e. As a control the surface of FC1 was activated with *N*-hydroxysuccinimide/1-ethyl-3-(3-dimethylaminopropyl)carbodiimide hydrochloride. Residual unreacted active ester groups were blocked with 1 M ethanolamine HCl, pH 8.5. NbStx2e1 was flowed over the chip surface with concentrations ranging from 0.122 to 250 nM in HBS buffer (10 mM HEPES, 150 mM NaCl, 1 mM EDTA, 0.005% Tween 20, pH 7.4) at a flow rate of 20 μl/min at 25 °C. Data were evaluated using the software BIAeval, and a Langmuir binding model with a 1:1 stoichiometry was fitted to the data, from which the rate constants k_{on} and k_{off} and the dissociation constant K_D were obtained.

Complex Formation, crystallization, and Data Collection—The purified Stx2e toxoid was added to the purified NbStx2e1 in equimolar concentration and dialyzed against 20 mM Tris, pH 8.0. The dialyzed sample was then subjected to HisTrap FF column (GE Healthcare) purification. Prior to loading the sample onto the column, 1 M NaCl was added and then subjected to a 20 mM to 1 M imidazole linear gradient in 20 mM Tris, pH 8.0, 1 M NaCl. Fractions containing the Stx2e toxoid-NbStx2e1 complex, as judged by SDS-PAGE, were pooled and dialyzed against 20 mM Hepes, pH 8.0, 100 mM imidazole, 500 mM NaCl. The complex was concentrated to 12 mg/ml. Crystallization of Stx2e toxoid-NbStx2e1 complex was achieved at 20 °C by vapor diffusion with 0.5-μl sitting drops and a complex/well solution (0.5 M succinic acid, pH 7.0, 0.1 M Bistris propane, pH 7.0) ratio of 1:1 (v/v).

Structure Determination and Refinement—Single-crystal x-ray wavelength diffraction data were collected at 0.98-Å wavelength at the Diamond Light Source beamline I24. Data were indexed and processed to 2.82 Å resolution using XDS (19) (Table 1). The crystals belonged to the P 2_1 2_1 2 space group containing one Stx2e molecule and five NbStx2e1 molecules per asymmetric unit. Data were phased by molecular replacement (Phaser) (20) using the coordinates of the previously determined Stx2e structure (Protein Data Bank code 1QOH) (3) and a nanobody structure of NBKB6 (Protein Data Bank code 4AQ1) (21). The model was rebuilt and refined against the native data to 2.8 Å resolution using iterative cycles of the graphics program COOT (22) and Phenix refine (23), resulting in a final model with *R*- and free *R*-factors of 19.0 and 24.5, respectively. The model contains 1212 residues, 98% of which fall within the generally allowed regions of the Ramachandran plot (Table 1).

RESULTS

Selection of Stx2e-recognizing Nanobodies—To obtain nanobodies that recognize Stx2e, a llama was immunized with purified Stx2e toxoid from Oanh *et al.* (5). The PCR fragments of the nanobody repertoire generated from the llama lymphocyte's cDNAs were cloned into the phage display vector pMES4 (17). A nanobody library of 2.5×10^7 transformants was obtained with an insert rate of at least 87% as determined by PCR. Eight Stx2e-recognizing nanobodies were identified through two successive rounds of panning. The experimental panning conditions were similar to those reported by Ghahroudi *et al.* (24). Amino acid sequence analysis revealed that these nanobodies belong to six unique families on the basis of differences in their complementarity-determining region CDR3 (Fig. 1).

The production of selected nanobodies as soluble His-tagged proteins was achieved after transforming the corresponding pMES4 vector carrying the nanobody genes in *E. coli* WK6 cells. Periplasmic extract of nanobodies carrying a C-terminal His tag was purified by nickel-immobilized metal affinity chromatography. The produced nanobodies were found to be highly pure (>95%) as judged by Coomassie-stained SDS-PAGE (data not shown).

The purified nanobodies were tested in ELISA to confirm their capability to recognize Stx2e toxoid. The ELISA results confirmed that all of the eight nanobodies recognized Stx2e toxoid at varying degrees in a dose-dependent manner (Fig. 2). Four of these nanobodies, NbStx2e1, NbStx2e2, NbStx2e3, and

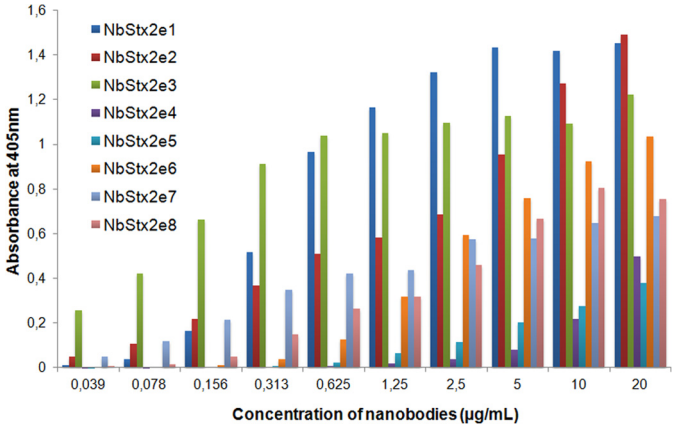

FIGURE 2. **Specificity of purified nanobodies to Stx2e toxoid.** The purified nanobodies were titrated in an indirect ELISA against purified Stx2e toxoid at 2 μg/ml. All of the eight nanobodies recognized the Stx2e toxoid at varying degrees in a dose-dependent manner.

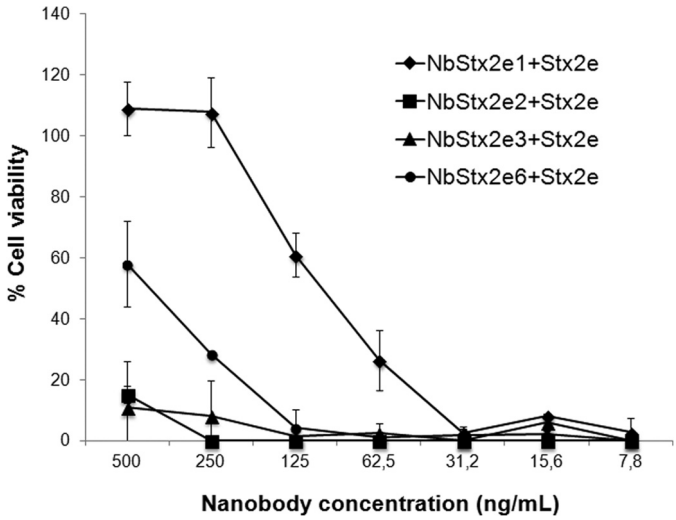

FIGURE 3. **Protection of Vero cells killing by Stx2e in the presence of nanobodies.** The percentage of Vero cell viability in the presence of NbStx2e1, NbStx2e2, NbStx2e3, or NbStx2e6 (nanobody) at varying concentrations was calculated using the formula, (A_{595} of nanobody and Stx2e − A_{595} with Stx2e only)/(A_{595} of nanobody only − A_{595} with Stx2e only) × 100. Experiments were repeated twice. Data are representative of replicate experiments presented as sample means ± S.E. (*error bars*).

NbStx2e6, showed strong binding to Stx2e toxoid and were selected for further characterization.

Protection of Stx2e Killing of Vero Cells by Nanobodies—The capability of the selected Stx2e toxoid-recognizing nanobodies to neutralize Stx2e toxin was assessed in a Vero cell-based neutralization assay. Of the nanobodies tested, NbStx2e2 and NbStx2e3 showed a lack of neutralizing potency at concentrations lower than 500 ng/ml. NbStx2e1 conferred the most potent neutralizing capacity in a dose-dependent manner with an IC_{50} value of 116 ng/ml (~8 nM) (95% confidence interval: 99–136 ng/ml; $R^2 = 0.97$) and followed by NbStx2e6 with an IC_{50} value of 265 ng/ml (21 nM) (95% confidence interval: 201–349 ng/ml; $R^2 = 0.96$) (Fig. 3). The promising neutralizing potency of NbStx2e1 prompted further elucidation of the neutralization mechanism of Stx2e by NbStx2e1 using x-ray crystallography.

Structural Insight into the Inhibitory Mechanism of NbStx2e1—For safety reasons and because of the need to produce protein in a large enough quantity for protein crystallography, we used Stx2e toxoid for the subsequent experiments. The complex between NbStx2e1 and the Stx2e toxoid was co-purified, and the structure was determined to a resolution of 2.8 Å (Table 1). Fig. 4 shows that Stx2e consists of a catalytic A subunit of 297 amino acids with *N*-glycosidase activity and a pentamer of B subunits (68 amino acids). The B subunit of Stx2e is essential to interact preferentially with the globotetraose (GalNAcβ1–3Galα1–4Galβ1–4Glc, Gb4) receptor, the latter present on the target cells as a glycolipid. The carboxyl end of the A subunit forms an α-helix that protrudes through the pore of the B-pentamer. In the earlier determined crystal structure of Stx2e, the last six residues of the A subunit of the Stx2e structure were disordered (3). In our crystal structure, only the last lysine residue from Stx2e remained undetectable in the electron density map, and it shows that the C-terminal part of the A subunit extends slightly outward from the B subunit pore (Fig. 4). Termination mutations introduced in two of the last six residues showed no effect on the proteolytic processing or enzymatic activity in Stx2 (25). Furthermore, the stretch of amino acid residues from position 242 to 258 of the A subunit of Stx2e is not visible in the electron density map.

TABLE 1
Data collection, crystal parameters, and refinement statistics for the complex between Stx2e and NbStx2e1

Beamline	I24 Diamond Light Source
Wavelength (Å)	0.98
Space group	P 2_1 2_1 2
a, *b*, *c* (Å)	191.8, 88.2, 100.7
Resolution (Å)	44.1-2.82 (3.01-2.82)[a]
R_{meas} (%)	19.4 (81.4)
$\langle I/\sigma I \rangle$	7.1 (2.7)
No. of unique reflections	42,054 (7496)
Completeness (%)	99.9 (100.0)
Multiplicity	6.0 (6.0)
R_{work}/R_{free} (%)[c,d]	19.0/24.5
Wilson *B*-factor	45.2
Average *B*-factor	
Protein (Å)	34.6
Solvent	NA[e]
Root mean square deviations	
Bond lengths (Å)	0.0105
Bond angles (degrees)	1.415
No. of atoms (except hydrogen)	9539
Residues in allowed regions (%) of Ramachandran plot	98
Protein Data Bank entry	4P2C

[a] Statistics for the outer resolution shell are given in parenthesis.
[b] $R_{meas} = \Sigma_h(nh/nh - 1)\Sigma l|Ihl - \langle Ih \rangle|/\Sigma_h\Sigma l\langle Ih \rangle$, where *nh* is the number of observations for reflection *h*, *Ihl* is the intensity for observation *l* of reflection *h*, and $\langle Ih \rangle$ is the average intensity for reflection *h*.
[c] $R_{work} = \Sigma_{hkl}||F_o| - |F_c\ 845||/\Sigma_{hkl}|F_o|$.
[d] R_{free} is defined as above but calculated for 5% of randomly chosen reflections that were excluded from the refinement.
[e] Not applicable.

For each B subunit of Stx2e, one NbStx2e1 is interacting in a head-to-head orientation (Fig. 4) and directly competing with the glycolipid receptor binding site on the B subunits (Figs. 5 and 6). Binding of Stx2e to the cell surface is a crucial initial step in the cytotoxicity, and the interaction of Stx2e with the target receptors on host tissue is obstructed by the steric hindrance the NbStx2e1 nanobodies impose upon binding. Each NbStx2e1 molecule is involved only in interactions with one single B subunit. When examining the interaction surface in more detail, all three CDRs of NbStx2e1 provide affinity and

specificity to the interaction with Stx2e (Fig. 5, *A* and *B*). On CDR1, the side chain of Arg-30 is forming hydrogen bonds with the side chains of Asp-16 and Thr-18 of the Stx2e B subunit. In addition, the main chain oxygen atom of Arg-30 forms a hydrogen bond with the side chain of Asn-31 of NbStx2e1. On the CDR2 loop, the main chain oxygen atom of Tyr-54 is interacting both with the side chain of Ser-53 and the main chain amide group of Asn-54. Ser-53 of the NbStx2e1 is forming a hydrogen bond with the side chain of Asn-31. On the CDR3 loop, Glu-100 forms hydrogen bonds with the side chains of Asn-31 and Arg-32, the carboxyl of Gly-102 forms a hydrogen bond with the main chain amide group of Trp-33, and finally the side chain hydroxyl group of Tyr-104 forms a hydrogen bond with the side chain of Asn-34. In addition, Trp-33 of the Stx2e B subunit is involved in a hydrophobic stacking interaction with the side chain of Tyr-104 (Fig. 5, *A* and *B*). The side chain of Asn-73, located on framework region 3, interacts with the carboxyl group of Gly-59.

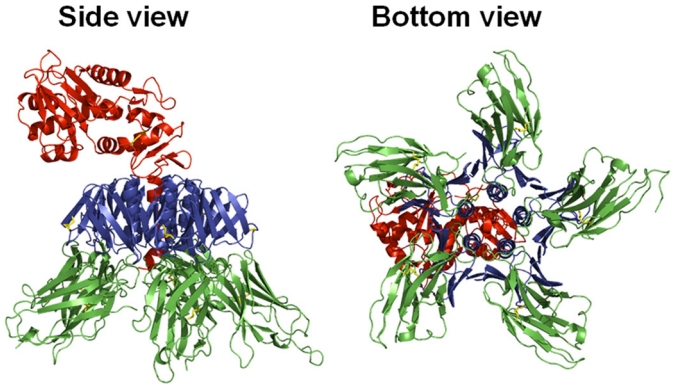

FIGURE 4. **Crystal structure of inhibitory NbStx2e1 in complex with the Stx2e toxoid.** Stx2e is composed of a catalytic A subunit (*red*) and a pentamer of glycolipid-binding B subunits (*blue*) that are arranged around a C-terminal α-helix from the A subunit. NbStx2e1 (*green*) is interacting with the B subunit in a way such that five molecules are able to bind simultaneously to Stx2e without any steric hindrance. The co-complex crystal structure reveals that NbStx2e1 is directly competing with the glycolipid binding pocket on the surface of Stx2e. NbStx2e1 and Stx2e are depicted in a schematic representation. Disulfide bridges are depicted in a *stick model* and *colored yellow*.

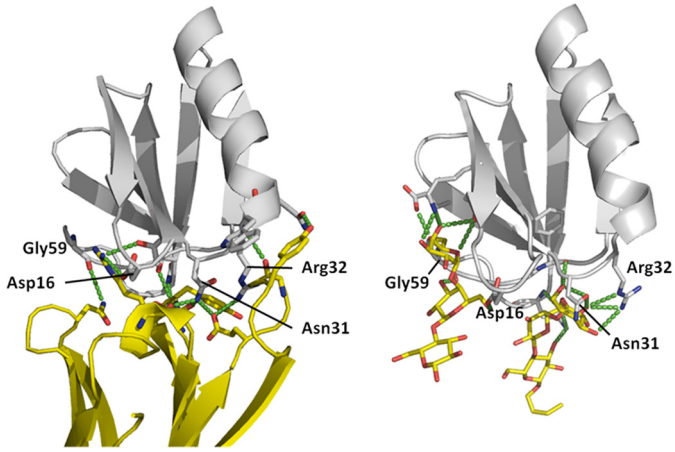

FIGURE 6. **NbStx2e1 directly competes with the sugar binding site on the Stx2e surface.** Shown is a comparison of the binding site of NbStx2e1 (*left*) and globotriaose (*Gb3*) (*right*) on the surface of the B subunit of Stx2e. Multiple residues on the Stx2e surface can be seen to interact both with NbStx2e1 and globotriaose, and these residues are named. NbStx2e1 thus directly competes with the glycan binding site of Stx2e. The B subunit of Stx2e is depicted in a schematic representation and *colored gray*, whereas NbStx2e1 and globotriaose are depicted in *schematic* and *stick representations*, respectively, and *colored yellow*. Interacting residues are shown in a *stick model* with oxygen and nitrogen atoms *colored red* and *blue*, respectively. Hydrogen bonds are *highlighted* as *green dotted lines*. The structure of Stx2e in complex with Gb3 was obtained from the Protein Data Bank (accession code 2BOS).

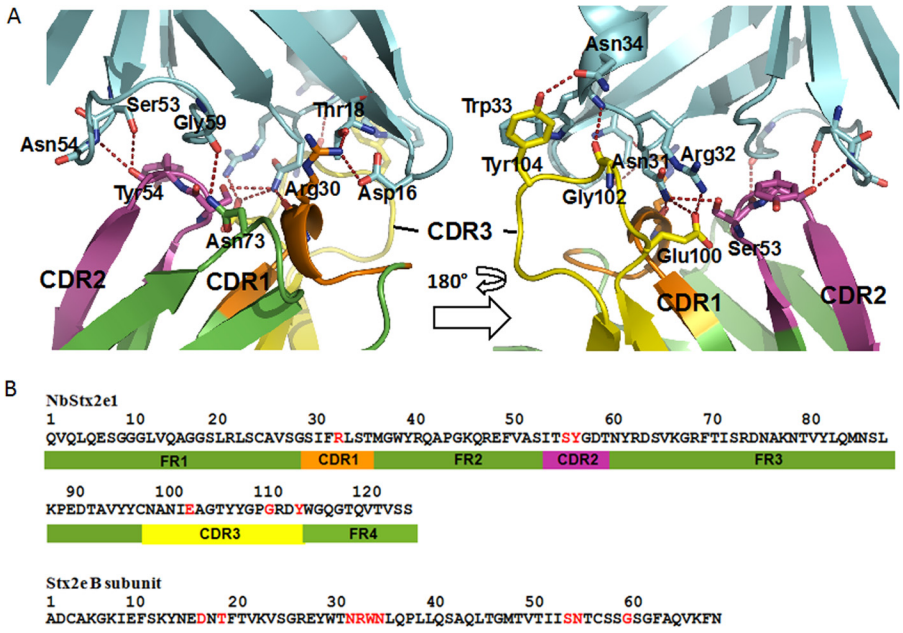

FIGURE 5. ***Close up* of the interaction between NbStx2e1 and Stx2e.** *A*, one NbStx2e1 molecule interacts with one B subunit of Stx2e. All three complementarity-determining regions (*CDR1–CDR3*) of NbStx2e1 are involved in the interaction. Amino acid residues important in binding are shown in a *stick model* and *named*. The interaction is mainly governed by the formation of stabilizing hydrogen bonds, although Trp-33 of the B subunit forms a hydrophobic stacking interaction with Tyr-104 of NbStx2e1. NbStx2e1 is *colored green*, and the Stx2e B subunit is *cyan*; CDR1–3 of NbStx2e1 are *colored orange*, *purple*, and *yellow*, respectively. Hydrogen bonds stabilizing the interaction are depicted as *red dashed lines*. *B*, amino acid sequence of NbStx2e1 and Stx2e B subunit. *Green boxes* indicate NbStx2e1 structural framework regions FR1–4; the complementarity-determining regions CDR1–3 of NbStx2e1 are represented in *orange*, *purple*, and *yellow boxes*, respectively. Interacting residues of NbStx2e1 and Stx2e are shown in *red*. The amino acid sequence of NbStx2e1 is *numbered* according to IMGT numbering (38).

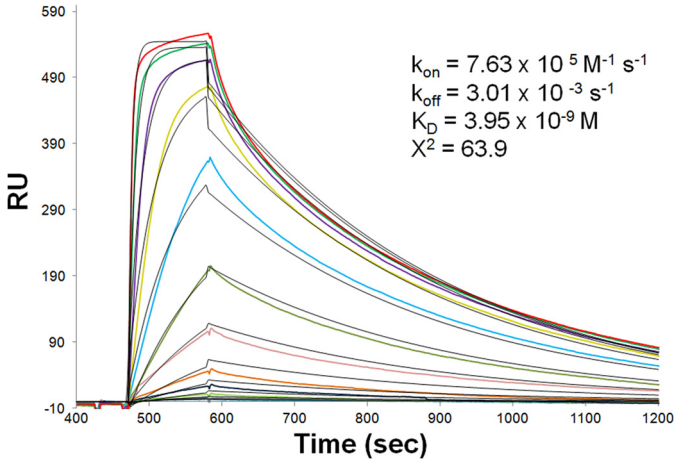

FIGURE 7. **NbStx2e1 interacts with high nanomolar affinity with Stx2e.** The interaction between NbStx2e1 and Stx2e was assayed using SPR. Sensorgrams were obtained of varying concentrations (0.122–250 nM) of NbStx2e1 injected over immobilized Stx2e. The curves were fitted using a 1:1 Langmuir binding model and demonstrated that NbStx2e1 recognizes the toxin in the low nanomolar range. *Fitted curves* are shown in *black*, whereas the original data are represented by the *colored curves*. *RU,* resonance units.

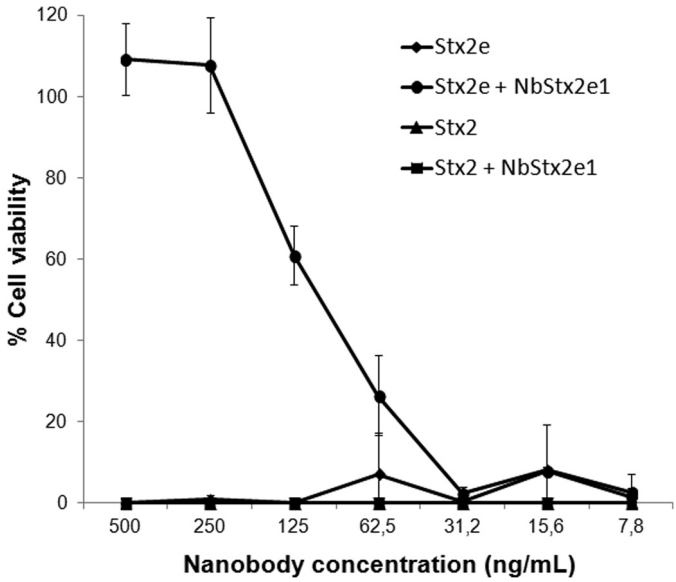

FIGURE 8. **Protection of Vero cell killing by Stx2 or Stx2e toxin in the presence of NbStx2e1.** The percentage of Vero cell viability in the presence or absence of NbStx2e1 at varying concentrations was calculated using the formula, (A_{595} of nanobody and Stx2e − A_{595} with Stx2e only)/(A_{595} of nanobody only − A_{595} with Stx2e only) × 100. Data are representative of replicate experiments presented as sample means ± S.E. Approximately 10 times the 50% cytotoxic dose (predetermined concentration; data not shown) of Stx2 or a total of 2 ng/ml Stx2e toxin was used for each sample.

Affinity of NbStx2e1 for Stx2e—The strength of the interaction between NbStx2e1 and Stx2e was quantified using SPR. Stx2e was covalently immobilized via its free amine groups, and multiple injections at different concentrations of NbStx2e1 revealed a binding profile with high association and low dissociation rates (Fig. 7). When fitted to a 1:1 binding model, an apparent K_D was determined of roughly 4 nM with k_{on} and k_{off} values of 7.63×10^5 M^{-1} s^{-1} and 3.01×10^{-3} s^{-1}, respectively. The nanomolar affinity interaction between Stx2e and NbStx2e1 corresponds to the potent neutralizing capacity of NbStx2e1 and further confirms the extensive hydrogen bond network, as observed in the structure of the Stx2e-NbStx2e1 complex.

DISCUSSION

Currently, there is no specific therapeutic agent available to prevent and treat infection by Shiga toxin-producing *E. coli* despite decades of research and development efforts. The role of antibiotic prophylaxis to prevent Shiga toxin-producing *E. coli* infection remains controversial because of the possibility of enhancing the production and release of Shiga toxins (26, 27). To date, immunotherapy remains a therapeutic approach of choice given that specific antibodies are capable of neutralizing preformed toxin (28). Moreover, by targeting preformed toxin, selection pressure is removed from the bacteria, reducing the chance of antibiotic resistance. There have been a number of murine or human mAbs against Shiga toxin developed over the years, as reviewed by Chow and Casadevall (28) and more recently an engineered multivalent Stx1/Stx2 cross-specific VHH (15). The majority of these neutralizing agents are B subunit-specific with a few exceptions that are A subunit-specific, namely mAbs 11E10 (7) and 5C12 (29). Despite a multitude of studies, the detailed molecular mechanism for inhibition of these neutralizing mAbs and VHH remains elusive.

Stx2e-producing strains of *E. coli* have been implicated as a causative agent of ED in neonatal piglets (30). ED is highly contagious and can result in neurological disorders, hemorrhagic lesions, and frequent fatal outcome. The high mortality rate in Stx2e-producing *E. coli*-infected pigs has a severe economic impact on the swine industry. The lack of effective therapeutic agents for treatment of ED and the prevalence of antibiotic-resistant porcine Stx2e-producing *E. coli* isolates signal an urgent need to develop new therapeutic approaches. It has been shown that immunization of piglets and sow with Stx2e toxoid resulted in protection against Stx2e toxin challenge (5). This suggests that Stx2e-neutralizing antibodies can be an effective treatment for ED. Furthermore, the highly conserved amino acid sequences (more than 99% identical) of Stx2e among the Stx2e-producing *E. coli* strains isolated from pigs with ED, humans, environment, and food (31–33) satisfy the essential criteria for its use as an immunotherapy target.

In this study, we generated a nanobody phage display library by immunizing a llama with Stx2e toxoid and isolated eight Stx2e-recognizing nanobodies. These nanobodies were expressed as soluble proteins in *E. coli*, and their dose-dependent interactions with Stx2e were confirmed using ELISA. Of the four nanobodies that showed strong recognition of Stx2e toxoid, NbStx2e1 exhibited the most potent neutralizing activity, with an IC_{50} value of 116 ng/ml (8 nm) against Stx2e toxin in a Vero cell cytotoxicity assay. The potent neutralizing activity of NbStx2e1 corresponded to the high affinity interaction (K_D = 4 nM) with Stx2e as measured by SPR. We also further showed that NbStx2e1 was specific for Stx2e and was not able to neutralize Shiga toxin variant Stx2 (Fig. 8).

To gain molecular insight into the neutralization mechanism of NbStx2e1, crystallization of the NbStx2e1-Stx2e complex was performed. Our crystal structure of this complex uncovered that NbStx2e1 sterically prevents the binding of Stx2e to host cell receptor by direct interaction with the Stx2e B subunit (Figs. 4 and 5). The NbStx2e1 epitope overlaps with the ligand-

binding site of the B subunit (Fig. 6). Mutational analysis showed that conserved Arg-32 and Gly-59 residues of the B subunit are pivotal for Stx1 and Stx2 cytotoxicity (34). Moreover, Gly-59 in the Stx2e B subunit has also been shown to be involved in trisaccharide binding (3). In corroboration with this finding, these residues indeed constitute part of the epitope recognized by NbStx2e1 (Fig. 6). Our findings provide the first structural evidence for the mechanism of inhibition of Stx2e by NbStx2e1 that will pave the way for future therapeutic use of nanobodies against Shiga toxins.

With respect to ED treatment, the potent NbStx2e1 identified in this study can potentially be expressed and delivered through animal feed, as exemplified by a recent study (35). In this study, anti-enterotoxigenic *E. coli* (anti-F4 fimbriae) nanobodies were grafted onto the Fc part of porcine immunoglobulin IgA and expressed in *Arabidopsis thaliana* seeds. Ground seeds were mixed with piglet starter feed and conferred oral passive protection to weaned piglets against enterotoxigenic *E. coli* infection (35). Alternatively, intravenous administration of NbStx2e1 is a possibility. For this approach, given the small size of the nanobody and the lack of the Fc region, modifications may be required to further improve NbStx2e1 serum half-life. Several methods have been reported, including grafting of nanobodies onto porcine immunoglobulin (36) and PEGylation, the covalent attachment of polyethylene glycol polymer chains to nanobodies, to reduce rapid blood clearance in guinea pigs (37).

In summary, we have isolated and expressed eight nanobodies that recognize Stx2e. We have identified and characterized these nanobodies, and NbStx2e1 was found to confer potent neutralization capability against Stx2e cytotoxicity through high affinity interaction with the B subunit of Stx2e. The crystal structure of the NbStx2e1-Stx2e complex unambiguously uncovers the position and orientation of the bound NbStx2e1 to the B subunit of Stx2e. The intrinsic properties of nanobodies (high target affinity and specificity, stability, and ease of expressing at high yields in recombinant organisms) make them an attractive therapeutic agent.

Acknowledgment—We are grateful to the beamline staff of I04 at the Diamond Light Source (UK) for support with the data collection and processing.

REFERENCES

1. Gyles, C. L. (2007) Shiga toxin-producing *Escherichia coli*: an overview. *J. Anim. Sci.* **85,** E45–E62
2. Imberechts, H., De Greve, H., and Lintermans, P. (1992) The pathogenesis of edema disease in pigs. A review. *Vet. Microbiol.* **31,** 221–233
3. Ling, H., Pannu, N. S., Boodhoo, A., Armstrong, G. D., Clark, C. G., Brunton, J. L., and Read, R. J. (2000) A mutant Shiga-like toxin IIe bound to its receptor Gb(3): structure of a group II Shiga-like toxin with altered binding specificity. *Structure* **8,** 253–264
4. DeGrandis, S., Law, H., Brunton, J., Gyles, C., and Lingwood, C. A. (1989) Globotetraosylceramide is recognized by the pig edema disease toxin. *J. Biol. Chem.* **264,** 12520–12525
5. Oanh, T. K., Nguyen, V. K., De Greve, H., and Goddeeris, B. M. (2012) Protection of piglets against Edema disease by maternal immunization with Stx2e toxoid. *Infect. Immun.* **80,** 469–473
6. Nakao, H., Kiyokawa, N., Fujimoto, J., Yamasaki, S., and Takeda, T. (1999) Monoclonal antibody to Shiga toxin 2 which blocks receptor binding and neutralizes cytotoxicity. *Infect. Immun.* **67,** 5717–5722
7. Perera, L. P., Marques, L. R., and O'Brien, A. D. (1988) Isolation and characterization of monoclonal antibodies to Shiga-like toxin II of enterohemorrhagic *Escherichia coli* and use of the monoclonal antibodies in a colony enzyme-linked immunosorbent assay. *J. Clin. Microbiol.* **26,** 2127–2131
8. Krautz-Peterson, G., Chapman-Bonofiglio, S., Boisvert, K., Feng, H., Herman, I. M., Tzipori, S., and Sheoran, A. S. (2008) Intracellular neutralization of shiga toxin 2 by an a subunit-specific human monoclonal antibody. *Infect. Immun.* **76,** 1931–1939
9. Mukherjee, J., Chios, K., Fishwild, D., Hudson, D., O'Donnell, S., Rich, S. M., Donohue-Rolfe, A., and Tzipori, S. (2002) Production and characterization of protective human antibodies against Shiga toxin 1. *Infect. Immun.* **70,** 5896–5899
10. Smith, M. J., Carvalho, H. M., Melton-Celsa, A. R., and O'Brien, A. D. (2006) The 13C4 monoclonal antibody that neutralizes Shiga toxin Type 1 (Stx1) recognizes three regions on the Stx1 B subunit and prevents Stx1 from binding to its eukaryotic receptor globotriaosylceramide. *Infect. Immun.* **74,** 6992–6998
11. Kimura, T., Co, M. S., Vasquez, M., Wei, S., Xu, H., Tani, S., Sakai, Y., Kawamura, T., Matsumoto, Y., Nakao, H., and Takeda, T. (2002) Development of humanized monoclonal antibody TMA-15 which neutralizes Shiga toxin 2. *Hybrid Hybridomics* **21,** 161–168
12. López, E. L., Contrini, M. M., Glatstein, E., González Ayala, S., Santoro, R., Allende, D., Ezcurra, G., Teplitz, E., Koyama, T., Matsumoto, Y., Sato, H., Sakai, K., Hoshide, S., Komoriya, K., Morita, T., Harning, R., and Brookman, S. (2010) Safety and pharmacokinetics of urtoxazumab, a humanized monoclonal antibody, against Shiga-like toxin 2 in healthy adults and in pediatric patients infected with Shiga-like toxin-producing *Escherichia coli*. *Antimicrob. Agents Chemother.* **54,** 239–243
13. Hamers-Casterman, C., Atarhouch, T., Muyldermans, S., Robinson, G., Hamers, C., Songa, E. B., Bendahman, N., and Hamers, R. (1993) Naturally occurring antibodies devoid of light chains. *Nature* **363,** 446–448
14. Muyldermans, S. (2013) Nanobodies: natural single-domain antibodies. *Annu. Rev. Biochem.* **82,** 775–797
15. Tremblay, J. M., Mukherjee, J., Leysath, C. E., Debatis, M., Ofori, K., Baldwin, K., Boucher, C., Peters, R., Beamer, G., Sheoran, A., Bedenice, D., Tzipori, S., and Shoemaker, C. B. (2013) A single VHH-based toxin neutralizing agent and an effector antibody protects mice against challenge with Shiga toxins 1 and 2. *Infect. Immun.* **81,** 4592–4603
16. Strockbine, N. A., Jackson, M. P., Sung, L. M., Holmes, R. K., and O'Brien, A. D. (1988) Cloning and sequencing of the genes for Shiga toxin from *Shigella dysenteriae* type 1. *J. Bacteriol.* **170,** 1116–1122
17. Pardon, E., Laeremans, T., Triest, S., Rasmussen, S. G., Wohlkönig, A., Ruf, A., Muyldermans, S., Hol, W. G., Kobilka, B. K., and Steyaert, J. (2014) A general protocol for the generation of Nanobodies for structural biology. *Nat. Protoc.* **9,** 674–693
18. Conrath, K. E., Lauwereys, M., Galleni, M., Matagne, A., Frère, J. M., Kinne, J., Wyns, L., and Muyldermans, S. (2001) β-Lactamase inhibitors derived from single-domain antibody fragments elicited in the camelidae. *Antimicrob. Agents Chemother.* **45,** 2807–2812
19. Otwinowski, Z., and Minor, W. (1997) Processing of x-ray diffraction data collected in oscillation mode. *Methods Enzymol.* **276,** 307–326
20. McCoy, A. J., Grosse-Kunstleve, R. W., Adams, P. D., Winn, M. D., Storoni, L. C., and Read, R. J. (2007) Phaser crystallographic software. *J. Appl. Crystallogr.* **40,** 658–674
21. Baranova, E., Fronzes, R., Garcia-Pino, A., Van Gerven, N., Papapostolou, D., Péhau-Arnaudet, G., Pardon, E., Steyaert, J., Howorka, S., and Remaut, H. (2012) SbsB structure and lattice reconstruction unveil Ca^{2+} triggered S-layer assembly. *Nature* **487,** 119–122
22. Emsley, P., and Cowtan, K. (2004) Coot: model-building tools for molecular graphics. *Acta Crystallogr. D Biol. Crystallogr.* **60,** 2126–2132
23. Afonine, P. V., Grosse-Kunstleve, R. W., Echols, N., Headd, J. J., Moriarty, N. W., Mustyakimov, M., Terwilliger, T. C., Urzhumtsev, A., Zwart, P. H., and Adams, P. D. (2012) Towards automated crystallographic structure refinement with phenix.refine. *Acta Crystallogr. D Biol. Crystallogr.* **68,** 352–367
24. Arbabi Ghahroudi, M., Desmyter, A., Wyns, L., Hamers, R., and Muylder-

mans, S. (1997) Selection and identification of single domain antibody fragments from camel heavy-chain antibodies. *FEBS Lett.* **414,** 521–526
25. Haddad, J. E., al-Jaufy, A. Y., and Jackson, M. P. (1993) Minimum domain of the Shiga toxin A subunit required for enzymatic activity. *J. Bacteriol.* **175,** 4970–4978
26. Grif, K., Dierich, M. P., Karch, H., and Allerberger, F. (1998) Strain-specific differences in the amount of Shiga toxin released from enterohemorrhagic *Escherichia coli* O157 following exposure to subinhibitory concentrations of antimicrobial agents. *Eur. J. Clin. Microbiol. Infect. Dis.* **17,** 761–766
27. Walterspiel, J. N., Ashkenazi, S., Morrow, A. L., and Cleary, T. G. (1992) Effect of subinhibitory concentrations of antibiotics on extracellular Shiga-like toxin I. *Infection* **20,** 25–29
28. Chow, S. K., and Casadevall, A. (2012) Monoclonal antibodies and toxins: a perspective on function and isotype. *Toxins* **4,** 430–454
29. Mukherjee, J., Chios, K., Fishwild, D., Hudson, D., O'Donnell, S., Rich, S. M., Donohue-Rolfe, A., and Tzipori, S. (2002) Human Stx2-specific monoclonal antibodies prevent systemic complications of *Escherichia coli* O157:H7 infection. *Infect. Immun.* **70,** 612–619
30. MacLeod, D. L., Gyles, C. L., and Wilcock, B. P. (1991) Reproduction of edema disease of swine with purified Shiga-like toxin-II variant. *Vet. Pathol.* **28,** 66–73
31. Beutin, L., Krüger, U., Krause, G., Miko, A., Martin, A., and Strauch, E. (2008) Evaluation of major types of Shiga toxin 2E-producing *Escherichia coli* bacteria present in food, pigs, and the environment as potential pathogens for humans. *Appl. Environ. Microbiol.* **74,** 4806–4816
32. Oanh, T. K., Nguyen, V. K., Do, T. N., Goddeeris, B. M., and De Greve, H. (2010) *Escherichia coli* strains causing edema disease in northern Vietnam share an identical verotoxin 2e. *Trop. Anim. Health Prod.* **42,** 1797–1804
33. Vernozy-Rozand, C., Montet, M. P., Bertin, Y., Trably, F., Girardeau, J. P., Martin, C., Livrelli, V., and Beutin, L. (2004) Serotyping, stx2 subtyping, and characterization of the locus of enterocyte effacement island of shiga toxin-producing *Escherichia coli* and *E. coli* O157:H7 strains isolated from the environment in France. *Appl. Environ. Microbiol.* **70,** 2556–2559
34. Perera, L. P., Samuel, J. E., Holmes, R. K., and O'Brien, A. D. (1991) Identification of three amino acid residues in the B subunit of Shiga toxin and Shiga-like toxin type II that are essential for holotoxin activity. *J. Bacteriol.* **173,** 1151–1160
35. Virdi, V., Coddens, A., De Buck, S., Millet, S., Goddeeris, B. M., Cox, E., De Greve, H., and Depicker, A. (2013) Orally fed seeds producing designer IgAs protect weaned piglets against enterotoxigenic *Escherichia coli* infection. *Proc. Natl. Acad. Sci. U.S.A.* **110,** 11809–11814
36. Harmsen, M. M., Van Solt, C. B., Fijten, H. P., and Van Setten, M. C. (2005) Prolonged *in vivo* residence times of llama single-domain antibody fragments in pigs by binding to porcine immunoglobulins. *Vaccine* **23,** 4926–4934
37. Harmsen, M. M., van Solt, C. B., Fijten, H. P., van Keulen, L., Rosalia, R. A., Weerdmeester, K., Cornelissen, A. H., De Bruin, M. G., Eblé, P. L., and Dekker, A. (2007) Passive immunization of guinea pigs with llama single-domain antibody fragments against foot-and-mouth disease. *Vet. Microbiol.* **120,** 193–206
38. Lefranc, M. P., Pommié, C., Ruiz, M., Giudicelli, V., Foulquier, E., Truong, L., Thouvenin-Contet, V., and Lefranc, G. (2003) IMGT unique numbering for immunoglobulin and T cell receptor variable domains and Ig superfamily V-like domains. *Dev. Comp. Immunol.* **27,** 55–77